Received: 28 April 2023 | Revised: 4 October 2023 | Accepted: 12 October 2023

DOI: 10.1049/rsn2.12498

IET Radar, Sonar & Navigation

The Institution of Engineering and Technology WILEY

ORIGINAL RESEARCH

Radar signatures of sea lions at K-band and W-band

Samiur Rahman[1] | Aleksanteri B. Vattulainen[1] | Duncan A. Robertson[1] | Ryan Milne[2]

[1]School of Physics and Astronomy, University of St Andrews, St Andrews, Scotland

[2]Sea Mammal Research Unit, University of St Andrews, St Andrews, Scotland

Correspondence

Samiur Rahman, School of Physics & Astronomy, University of St Andrews, North Haugh, KY16 9SS, St Andrews, Scotland.
Email: sr206@st-andrews.ac.uk

Funding information

Engineering and Physical Sciences Research Council, Grant/Award Number: EP/S032851/1

Abstract

The millimetre wave radar signatures of sea lions collected from three animals in the outdoor seal pool available at the Sea Mammal Research Unit in St Andrews in the Autumn of 2021 is reported. The objective is to study the radar amplitude and Doppler signatures of the animals when their full body or part thereof is above water, which is important for the application of autonomous marine navigation. The data was collected using 24 GHz (K-band) and 77 GHz (W-band) Frequency Modulated Continuous Wave radars with linear polarisation. It has been demonstrated that the sea lions were very clearly detected by the radars with Signal to Noise Ratio greater than 30 dB at a range of 40 m. The calculated modal radar cross section (RCS) of the sea lions in HH polarisation at 24 and 77 GHz vary from −48 to −26 dBsm and −48 to −28 dBsm respectively, corresponding to the different body parts and the amount of exposure to the radar beam. In VV polarisation, the modal RCS value range is from −49 to −26 dBsm and −49 to −22 dBsm respectively. The corresponding maximum RCS and the Cumulative Distribution Function results are also reported.

KEYWORDS

radar, radar cross-sections, sea clutter

1 | INTRODUCTION

Due to the advancements in commercial millimetre wave chipset technology for the automotive industry, radars operating at these frequencies are now being explored for autonomous marine vessels. Radar plays a key role as a sensor due to its ability to work in practically all weather conditions. Traditionally, most marine navigation radars operate in X-band. In comparison, higher microwave frequency (K-band) and millimetre wave (W-band) radars have the advantage of being comparatively more compact and lightweight whilst simultaneously offering high resolution due to wide bandwidths and narrow beams. Such advantages mean they can provide detailed information of the surroundings, as required for vessel autonomy.

One of the main challenges for an autonomous marine vessel sensor is to detect and avoid large air breathing aquatic or semi-aquatic mammals (i.e. whales), which are protected species. To construct a reliable autonomous system, it is then very important to understand the radar signatures of such creatures in detail. This information can then be used for automatic target detection algorithm development. Radar systems have been used for detecting animals in various applications (avian biology, marine biology, entomological research etc.) [1]. Currently, studies of the radar signatures of sea mammals are very scarcely reported in the literature. In fact, reports on sea clutter data in general are very much confined within S-band, C-band and X-band, along with some limited Ka-band information [2]. In ref. [3], results of humpback whales detected by X-band radar at ~8 km range in the Mediterranean sea were shown. Radar detection and tracking of fin whales and *Stenella* dolphins up to 5.5 km at low sea states were also reported. In ref. [4], detection of whales with an X-band Furuno radar mounted on NOAA R/V MacArthur II ship was reported. The radar obtained was over 500 h of data in moderate to high sea states [5]. The ship carried a census team who were used for visual observations. A total of 42 visual observations were made, which were used

for radar data analysis. The radar target detection was done by simple Signal to Noise Ratio (SNR) thresholding. Various tracking algorithms were trialled, with no clear solution to overcome problems related to recurrent low SNR due to minimal exposure of the body (it was observed that the radar was not sensitive to whale blow). A fully coherent and polarimetric X-band radar was used to obtain data of southern right whales in Australia [6]. This was a land-based trial where the radar was positioned at the edge of a cliff at Nullarbor Plain. The data collection was performed over a wide range of incidence angles, so that the results can be applicable to ship-borne radars. Polarimetric domain analysis was performed on the collected radar data to enhance the contrast between the sea clutter and the target. In ref. [7], another X-band radar (Kelvin Hughes) was deployed on the Isle of Eday, northern Scotland (for a different application), which detected Atlantic orcas. The results showed a pair of orcas undertaking surface activity and were detected and tracked at ~7 km range. The radar was incoherent but was able to extract kinematic features for target classification. In ref. [8], the presence of marine mammals in the Mediterranean Sea were detected using an X-band radar. A contiguous Range-Time-Intensity (RTI) plot-based target classification algorithm was applied to the data, which was able to distinguish the observed 12 dolphins from other targets (ferries or sailing boats).

The aim of this study is to create a dataset of radar returns from different types of marine mammals at millimetre wave frequencies. The work is part of a wider project to assess the utility of sub-THz radars as sensors for marine autonomy, which requires knowledge of the radar signatures of objects on the sea surface, including sea mammals, which autonomous surface vessels would want to identify to make a manoeuvring decision. Radars operating at lower bands (K-band and W-band) are also of much interest due to their recent wider use and availability of components. The trial corresponding to this study was the first marine mammal radar data gathering, campaign, which will in future conduct further such expeditions under the Sub-THz Radar sensing of the Environment for future Autonomous Marine platforms (STREAM) project. Along with the details of the experimental trial, this paper reports on the amplitude and Doppler properties of the measured data, with the primary focus being the radar cross section (RCS) calculations of the animals for different activities at different polarisations. The initial results of this work were published in ref. [9]. In this study, more detailed results and analyses are added. Firstly, RCS and Doppler results of the sea lions at K-band are reported, whereas previously only the W-band results were shown. Also, data of the sea lions was fitted to the Swerling model along with calculations of the central moments of the Doppler spectra, which are all new results.

Section 2 of this article describes the experimental trial in detail. Section 3 contains the data analysis methodology and illustrates the obtained RCS and Doppler results of the sea lions at 24 and 77 GHz. Finally, future work and concluding remarks are stated in Section 4.

2 | EXPERIMENTAL SETUP

The data collection occurred on the 10th September, 2021 at the pool facility at the Sea Mammal Research Unit in St Andrews. Data were collected simultaneously with two radars operating at 24 GHz, named Blunderbuss [10] and 77 GHz, named FAROS-E [11].

The relevant radar parameters are shown in Table 1. The Blunderbuss radar actually has an output power of +25 dBm but during the trial, very strong returns from the surrounding clutter saturated the receiver chain so a 20 dB attenuator was used to suppress the signal, which still gave sufficient SNR for target detection at short range (~12 dB SNR at 40 m range for a −40 dBsm target). The FAROS-E radar was originally developed for real time drone detection, but was superseded by a 24 GHz variant for that application so the 77 GHz unit was modified for this particular field trial. This involved changing the antennas to wider beamwidth conical feedhorns to cover a wider arc length at short ranges. This was necessary as the targets were non-stationary and semi-cooperative. Additionally, the far field distance of the new antennas was quite small (~25 cm), appropriate for close range measurements. Waveguide straights were replaced by 90° waveguide twists to change the polarisation from V to H when needed. The anti-alias filter on the receive chain was set to suppress clutter beyond 40 m range, and the chirp parameters were adjusted to give a more suitable Doppler range. Radar calibration was performed a few days prior to the trial and confirmed the amplitude response was within 1–2 dB of theory, for both radars.

As shown in Figure 1a, the pool is 43 m long and 6 m wide. The radars were mounted on a tripod, 1.4 m above the ground, and pointed downwards by 5° along the long axis of the pool. The water and the ground were at the same level. The angle was optimised by carefully monitoring the clutter return coming from the surrounding metal bars at both sides and the

TABLE 1 24 GHz (blunderbuss) and 77 GHz radar (FAROS-E) parameters.

Parameter	Value	
Centre frequency (GHz)	24	76.5
Operating mode	FMCW	FMCW
Tx power (dBm)	+5	+25
Antenna beamwidth (one way)	11.2°	13°
Symmetric antenna gain (dBi)	24.5	22.2
Polarisation	HH, VV	HH, VV
Range resolution (cm)	60	20
Sampling rate (MHz)	3.125	17.8125
Chirp time (μs)	327.6	114.97
Chirp period (μs)	357.44	150.9
Chirp repetition frequency (kHz)	2.8	6.63
Max. unambiguous velocity (ms^{-1})	±8.84	±6.46

end of the pool, and then selecting the region with the lowest clutter return whilst pointing along the pool. The antenna boresight was then pointing at the water's surface at a range of approximately 16 m. Despite this arrangement, strong static clutter backscatter could not be avoided completely due to the very confined measurement area, as seen in Figure 1c, which shows the beam footprint of the Blunderbuss radar. Likewise, this also occurs with the FAROS-E radar due to its similar beampattern. Moving Target Indication (MTI) filtering had to be used during signal processing to eliminate these clutter returns. All the radar measurements were performed in staring mode. Three adult California sea lions (*Zalophus californianus*) were present in the pool during the data collection period (Figure 1b). There was one male (length 2.1 m, weight 122 kg) and two females (both length 1.8 m, weight ~80 kg). Radar data were collected for three different scenarios: (i) opportunistic data collection whenever the sea lions were partially above water during their natural swimming, (ii) dictating the sea lion movements in response to commands issued by their keeper (e.g. swimming with a flipper up) and (iii) commanding the male sea lion to jump clear of the water towards a ball suspended above the pool.

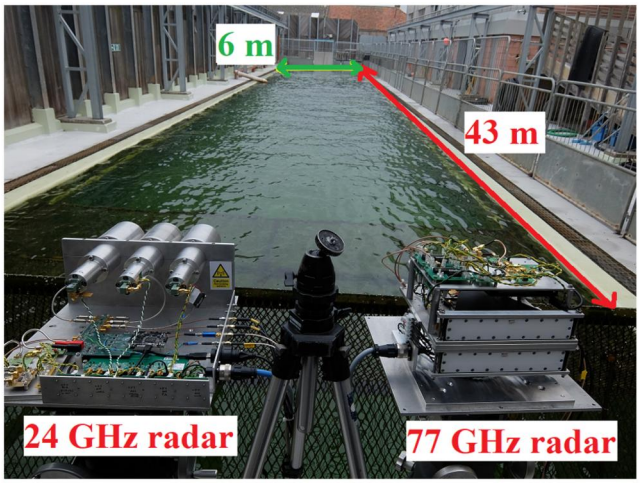

a

b

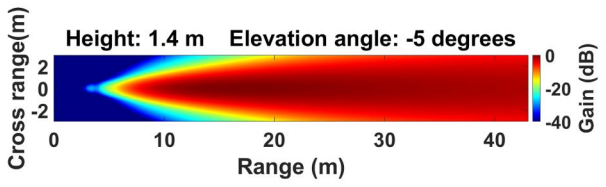

c

FIGURE 1 (a) Pool used for experimental trial at the Sea Mammal Research Unit, St Andrews, (b) The three sea lions whose radar signatures were measured, and (c) 24 GHz antenna beam footprint on the pool.

3 | RESULTS

As seen in Figure 2, the backscatter from the static clutter is very strong, in places greater than 60 dB above the radar noise floor of −93 dBm. Figure 2 also shows no significant difference in the pool water backscatter between HH and VV polarisation. This masks any target returns within the whole area of interest. To mitigate this, MTI processing was performed using the three-pulse canceller method [12]. It is an all-zero FIR filter with second order filter coefficients [1 −2 1]. The filtering was applied on the range processed complex data. Five consecutive chirps were used as each slow time sequence during the filtering process, which gave very good results in terms of the static clutter removal from the datasets. Figure 3 shows the effect of the MTI filter, where the presence of a target (one of the sea lions) is detected at ~15 m range after applying the filtering, which was previously buried under the clutter return. One practical issue was that the phase noise performance of Blunderbuss is not as good as FAROS-E. For strong target returns, MTI processing with the same parameters did not clean up the Blunderbuss range profiles as clearly as for FAROS-E so more consecutive chirps were used (10) for each time sequence along with first order coefficients [1 −1], which produced slightly better results. The difference in phase noise effect can be also observed in Figure 2. In the MTI filtered range profile plots, the noise floor adjacent to the sea

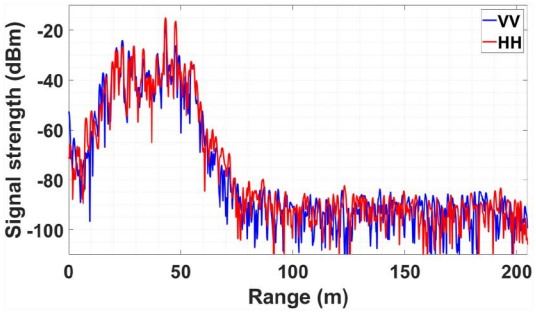

FIGURE 2 77 GHz radar range profiles in HH and VV, showing very strong clutter returns from the pool up to ~60 m range.

lion return is raised at 24 GHz. However, in the 77 GHz range plot, the noise floor remains flat at the presence of the bright target.

3.1 | RCS calculation

To estimate the RCS of the sea lions, RTI plots are generated. An area of interest is at first selected from the RTI plot corresponding to a specific action of the sea lion, where in all cases the sea lion activity is observed from coincident video. A total of five features were taken into consideration. These are head, head with upper body, vertical jump, horizontal jump and flipper. Range bins occupied by the target are then selected by finding the signal peaks. The return signal strength values are later converted to RCS values using the radar calibration curve. The intensity plots also reveal the kinematic information of the animals. Antenna beam pattern information (as seen in Figure 1c) was also incorporated for RCS estimations, as quite often the targets were off the antenna boresight. A flattop window has been used for the amplitude data processing. Due to the phase noise effect, the SNR of Blunderbuss was not always very good, especially for low level signals like returns from the flipper. For such cases the threshold value was adjusted manually to select the range bins of interest at 24 GHz, based on the noise level surrounding that region of interest. The overall RCS processing chain is as follows:

1. Select the area of interest from the RTI plot
2. Select the data points with amplitude above the given threshold—a value of 5 dB single shot SNR was used as a baseline but for some 24 GHz data affected by phase noise a threshold of 10–12 dB was used.
3. For a given range, the RCS is calculated using the following equation (all values in dB)

$$RCS_{\text{Target}} = P_{r_{\text{meas}}}\left(- P_{r_{\text{cal}}} - L_{\text{Ant}_{\text{gain}}} + RCS_{\text{cal target}}\right) \quad (1)$$

Here, RCS_{Target} is the measured sea lion RCS, $P_{r_{\text{meas}}}$ is the received power of the corresponding range bin, $P_{r_{\text{cal}}}$ is the received power of that range bin from the calibration curve of the radar and $RCS_{\text{cal target}}$ is the RCS of the calibration target that was used to obtain the calibration curve. The antenna loss factor $L_{\text{Ant}_{\text{gain}}}$ is also included due to the reason mentioned earlier.

Figure 4a shows the RTI plot of a 77 GHz HH polarised dataset without MTI filtering. The strong clutter backscatter

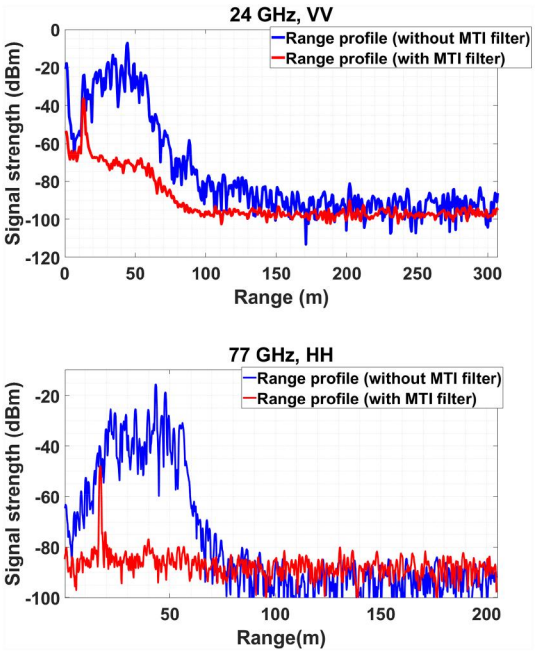

FIGURE 3 Effect of MTI filtering for surrounding static clutter suppression at 24 GHz, VV (top) and 77 GHz, HH (bottom). The return at ~15 m is from a sea lion.

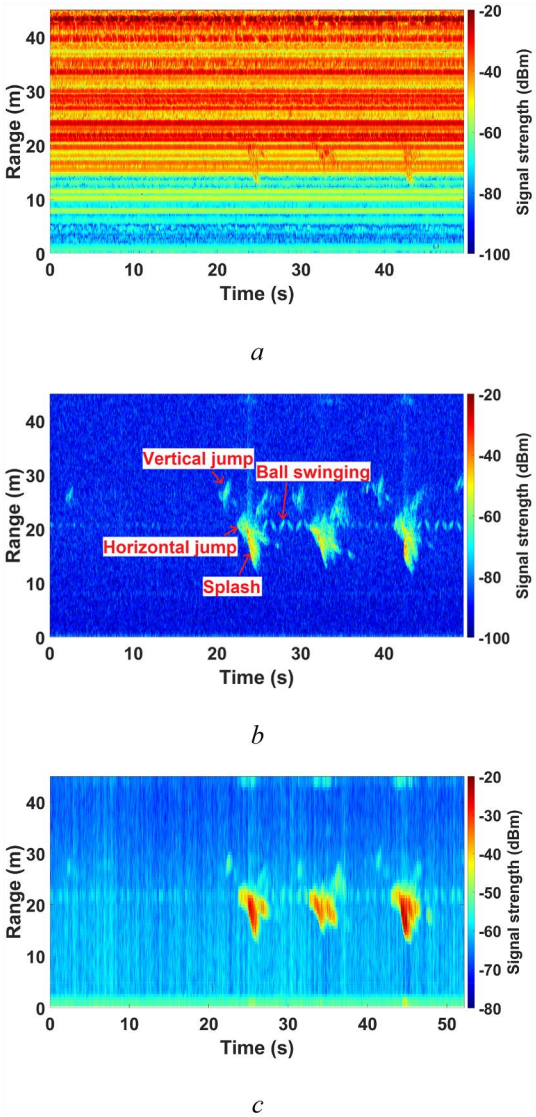

FIGURE 4 (a) RTI plot of HH polarised data without MTI filtering, (b), and after MTI filtering, revealing sea lion activities at 77 GHz, showing different activities, (c) Same MTI filtered RTI plot at 24 GHz HH.

obscures virtually all target information. Different types of sea lion activity are clearly revealed after the MTI processing, as illustrated in Figure 4b. The sea lions are detected with >20 dB SNR in most cases. At a time of ~20 s and range of ~30 m, the male sea lion jumped vertically to touch a ball attached to a wire a few metres above the pool. After ~2 s, right before re-entering the water, its position was orthogonal to the radar beam. The splash it made is clearly seen at ~25 s. The same manoeuvre was done two more times within the next 20 s. The periodic motion of the swinging ball is also observed in Figure 4b,c is the RTI plot of the same phenomenon at 24 GHz, with the same polarisation. The single shot IF noise floor of the radar is −80.1 dBm. It can be seen that the noise floor level on average is higher than that (−50 to −60 dBm), which is due to the phase noise. Still, the SNR of the target activities are good enough to pick out the relevant range bins for the RCS calculation. Figure 5 shows various example RTI plots from which different activities were traced. In Figure 5a, b, the returns from the heads of two sea lions can be observed in the first ~7 s, at 24 and 77 GHz respectively, in HH polarisation. In Figure 5c,d, the sea lion was swimming with its flipper up from 20 to 35 s, moving radially away from the radar. The polarisation here is VV. Understandably, the SNR in this case is quite small due to very small section of the body part being exposed to the antenna beam. In Figure 5e,f, the VV RTI plots of the 24 and 77 GHz data respectively show the return from the sea lion when it was approaching the radar with its head and upper body above the water, at ~13 s. The

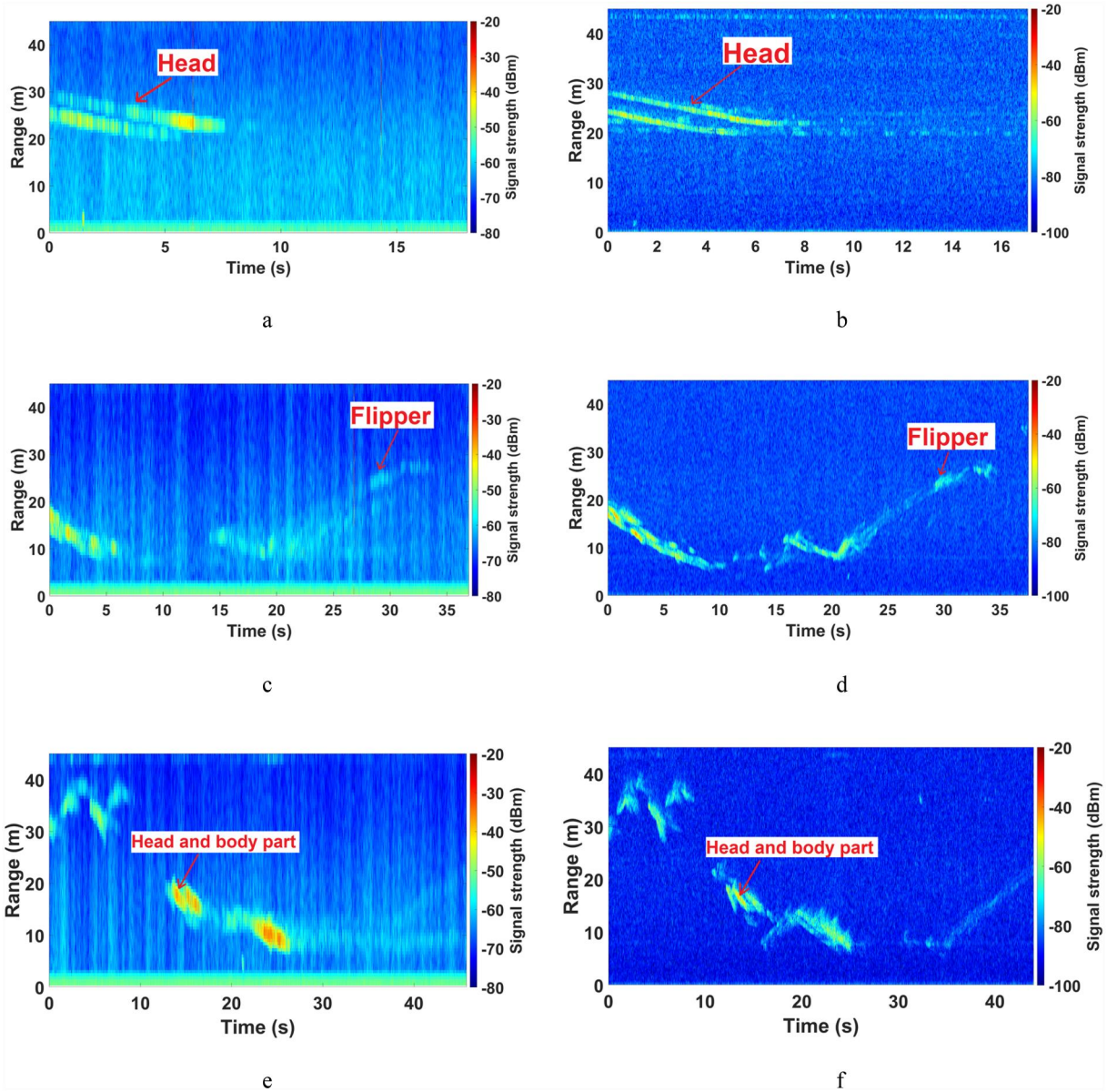

FIGURE 5 Example RTI plots used for RCS calculation, (a) HH RTI plot of two sea lion heads at 24 GHz, (b) HH RTI plot of two sea lions at 77 GHz, (c) VV RTI plot of a sea lion swimming with flipper up at 24 GHz, (d) VV RTI plot of a sea lion swimming with flipper up at 77 GHz, (e) VV RTI plot of a sea lion head and upper body part at 13 s at 24 GHz, (f) VV RTI plot of a sea lion head and upper body part at 13 s at 77 GHz.

wake created by the movement can also be seen on the side of the sea lion return.

The measured RCS values for all configurations are plotted in Figures 6 and 7. In the case of 24 GHz, the number of samples for each RCS plot generation varied from 200 to 500, whereas for 77 GHz, the range of number of samples is 1100–1500. The sample number being lower for 24 GHz is due to the more conservative thresholding to avoid data points

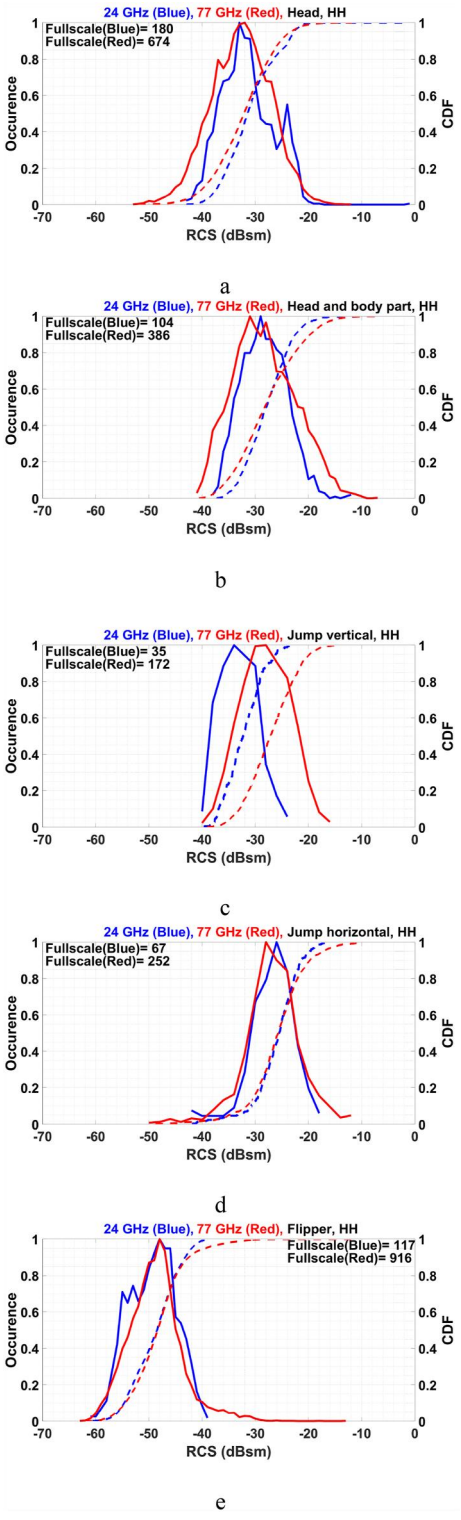

FIGURE 6 RCS histogram and CDF plots of different sea lion activities at HH polarisation at 24 and 77 GHz, (a) Head, (b) Head and body part, (c) Jump vertical, (d) Jump horizontal and (e) Flipper.

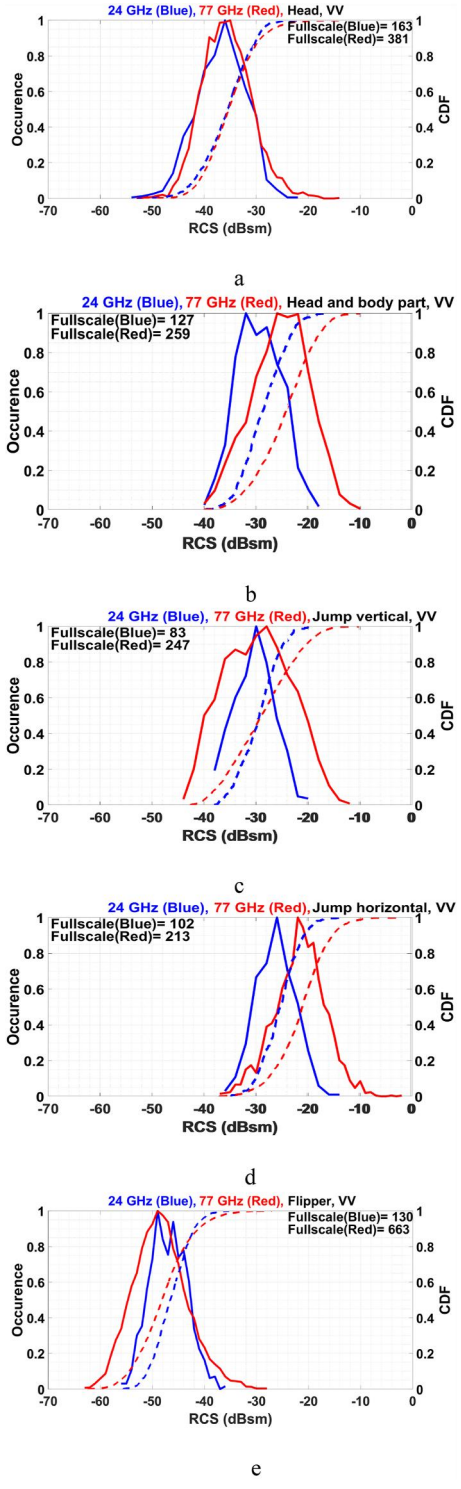

FIGURE 7 RCS histogram and CDF plots of different sea lion activities at VV polarisation at 24 and 77 GHz, (a) Head, (b) Head and body part, (c) Jump vertical, (d) Jump horizontal and (e) Flipper.

corresponding to phase noise and not actual target. Each plot overlays the 24 and 77 GHz RCS histograms along with the corresponding Cumulative Distribution Function (CDF) plots of an activity for a given polarisation. All the pertinent values (modal, maximum, 10% and 90% CDF points) are then listed in Table 2. The first observation made from the histogram plots is that the modal RCS values are quite similar at both frequencies, in both polarisations. There are few plots where 77 GHz shows a higher RCS than at 24 GHz. For instance, Figures 6c and 7b,d show the modal RCS values for 77 GHz are approximately 4–6 dB higher than the 24 GHz values. This may be due to the fact that while selecting the range bins from the 24 GHz RTI plots, the thresholding was more stringent to avoid spurious signals due to phase noise effects. Additionally, there might be slight target signal degradation at 24 GHz due to MTI processing, again for the same reason. Comparing the returns from HH and VV, it is also observed that the values for a given activity are within a few dBs, implying similar returns from both polarisations. The discrepancy of few a dBs may be due to slightly different exposure of the body parts in different data files. For instance, the orientation of the sea lion body during a jump was perhaps slightly different when the data was collected with one polarisation than the other. Hence, it is inferred that the overall RCS values of a sea lion are similar at both K-band and W-band.

The Swerling model [13], which is a variant of the chi-squared distribution, of the sea lion was explored. The jump horizontal activity in HH polarisation was selected for this (Figure 4) as that exposed the full body, which also corresponds to Figure 6d. Initial observation of the RCS variations in Figure 8a,b confirmed there was chirp-to-chirp RCS fluctuation. This suggests the target to be Swerling 2 or 4. The RCS histogram was plotted with the units converted to m^2, for Swerling model fit overlay. The continuous decaying nature of the histogram suggests the target to be Swerling 2, which means the target has multiple scatterers, without any of those being the dominant one. The following equation [13] was then used to generate the chi-squared Probability Density Function P_σ for the Swerling 2 model-

$$P(\sigma) = \frac{1}{\sigma_{\text{average}}} e^{\frac{-\sigma}{\sigma_{\text{average}}}} \quad (2)$$

Here, σ is the individual RCS values of the selected sea lion activity in m^2 and σ_{average} is the mean RCS. Figure 8c,d show that the model fits the measured data reasonably well, giving confidence in the target being Swerling 2.

3.2 | Doppler signatures

Doppler domain analysis is also performed to identify any characteristic signatures, with the expectation of observing some discernible features which discriminate a sea lion from a breaking wave. As there were no independent breaking waves during the measurements (i.e. waves which were not generated by the sea lions), a Doppler spectrogram of breaking waves from a beach trial conducted in the December of 2020 is used here for comparison. The W-band data were collected from a circularly polarised 94 GHz radar [14]. In Figure 9, a spectrogram of three consecutive breaking waves is demonstrated, where the waves are receding from the radar. Diffuse distributions lasting about 2 s are observed in the Doppler signatures of the waves. The corresponding Doppler spectra in Figure 9b illustrates this distribution, Full Width Half Maximum (FWHM) being relatively larger than the sea lion spectra. For comparison, Figure 10a is a 24 GHz spectrogram plotted for the event when the male sea lion was commanded to jump clear of the water, to touch a ball suspended ~3 m above the surface by a rope. The data were collected in HH polarisation here. The sea lion jumped three times causing big splashes when re-entering the water. Very strong Doppler returns from the three splashes are clearly seen. For better visualisation, Figure 10b is the spectrogram of the same event at 77 GHz. The Doppler features are clearly observed here as well. Figure 10c shows a zoomed in version of the 77 GHz plot, covering the 35–47 s period. Here, the dispersed distribution from the water splash is seen, akin to Figure 8 but with a larger intensity, as the breaking waves in Figure 8 were at low sea state (0 or 1). The Doppler return from the jumping sea lion is quite distinct from the breaking wave, appearing as a very narrow line due to the absence of any micro-Doppler component. This demonstrates that the Doppler information has the potential to be used for calculating statistical features for target classification

TABLE 2 RCS measurements summary.

	Average modal RCS (dBsm)				Maximum RCS (dBsm)				Average CDF 10% and 90% points (dBsm)			
	HH		VV		HH		VV		HH		VV	
Activity	24 GHz	77 GHz	24 GHz	77 GHz	24 GHz	77 GHz	24 GHz	77 GHz	24 GHz	77 GHz	24 GHz	77 GHz
Head	−32.5	−32	−36	−35	−20	−18	−24	−18	−38, −22	−42, −22	−42, −31	−43, −25
Head and body part	−29	−31	−32	−26	−12	−10	−22	−10	−35, −20	−37, −18	−35, −22	−34, −16
Jump vertical	−34	−28	−30	−28	−24	−16	−20	−12	−38, −26	−35, −19	−36, −23	−39, −22
Jump horizontal	−26	−28	−26	−22	−18	−12	−22	−9	−38, −20	−40, −16	−31, −19	−30, −14
Flipper	−48	−48	−49	−49	−39	−30	−36	−31	−56, −40	−42, −40	−52, −40	−56, −39

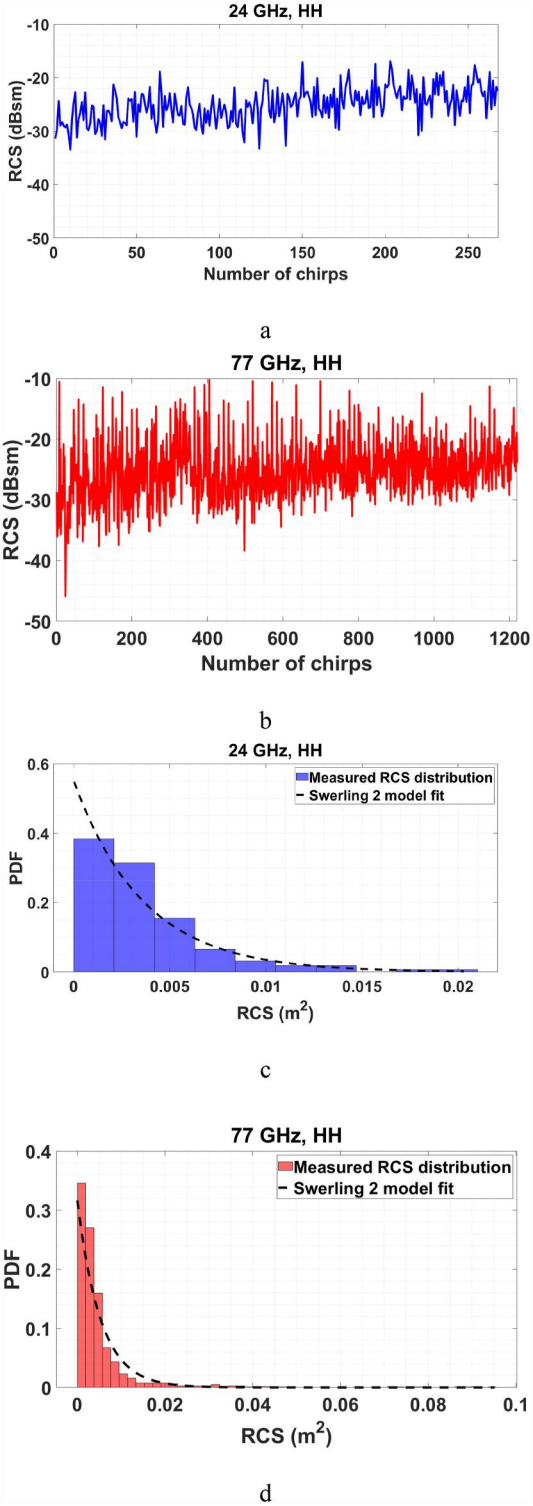

FIGURE 8 RCS fluctuation and Swerling model fit of the sea lion horizontal jump, (a) RCS fluctuation at 24 GHz, (b) RCS fluctuation at 77 GHz, (c) RCS histogram with Swerling 2 target model overlayed at 24 GHz, (c) RCS histogram with Swerling 2 target model overlayed at 77 GHz.

training. The sinusoidal pattern is the return from the swinging ball. The sinusoidal pattern increases in amplitude (increased velocity range) after the splash, from around 44 s.

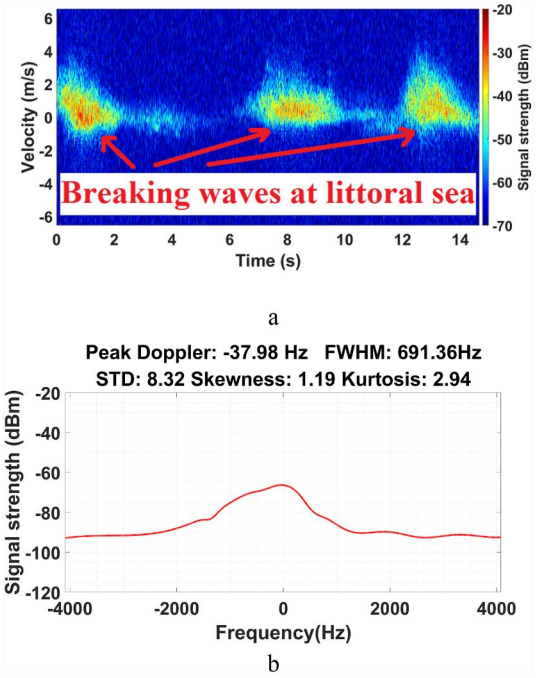

FIGURE 9 (a) 94 GHz Doppler spectrogram of receding breaking waves at littoral sea, (b) Doppler spectra and central moment values of the first breaking wave at 0–2 s.

This is because the ball started swinging faster due to the push by the sea lion at the jump apex. Figures 11 and 12 illustrate examples of the Doppler signatures from only parts of the sea lion body, specifically Doppler spectrograms and spectra from a flipper (Figure 11) and head (Figure 12), at both frequencies. A first order high pass filter was applied to the data before generating the spectra to suppress the zero Doppler return from the stationary targets. From the Doppler spectra, the peak Doppler, FWHM, standard deviation, skewness and kurtosis are calculated to determine the statistical properties. As mentioned before, the FWHM values of the sea lion Doppler spectra are smaller than the breaking wave spectra in Figure 9. In Figure 12d, the peak near zero Doppler is likely to be residue after the high pass filter. A second order filter suppresses that better but also suppresses the low Doppler return corresponding to the sea lion (body or wave generated by movement). These statistical values can be used for marine target classification or anomaly detection. Further analysis comparing the Doppler statistics of the sea lions to that of sea clutter, for the purpose of target discrimination, is being performed and will be reported in a separate publication.

4 | CONCLUSION

To the best of the authors' knowledge, this paper shows the first reported K-band and W-band radar signatures of sea lions and indeed of any marine mammal. The trial was conducted in an enclosed and controlled environment, ensuring

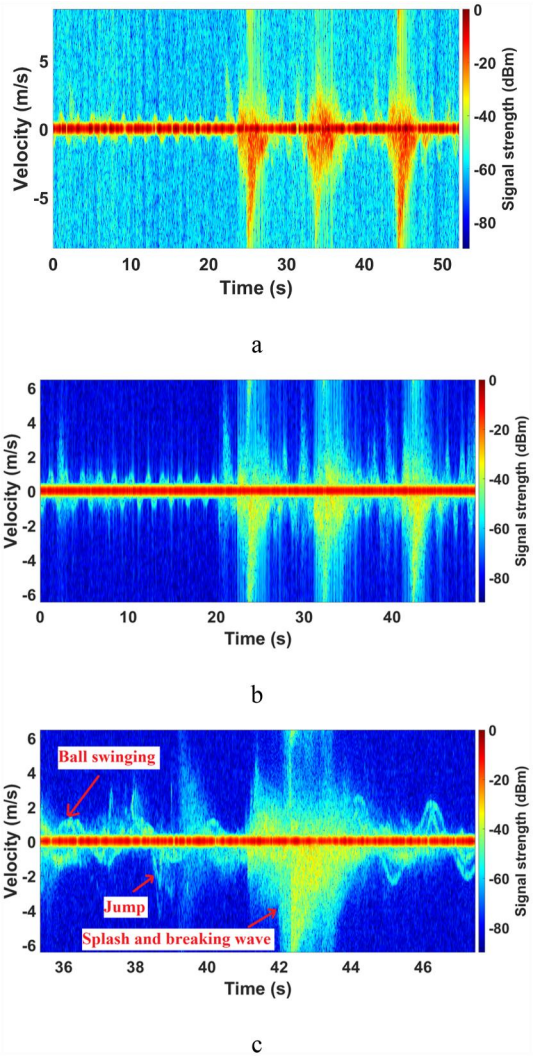

FIGURE 10 (a) Doppler spectrogram plot of a sea lion jumping clear of the water at 24 GHz, (b) the same event at 77 GHz, (c) zoomed in version of the event at 77 GHz.

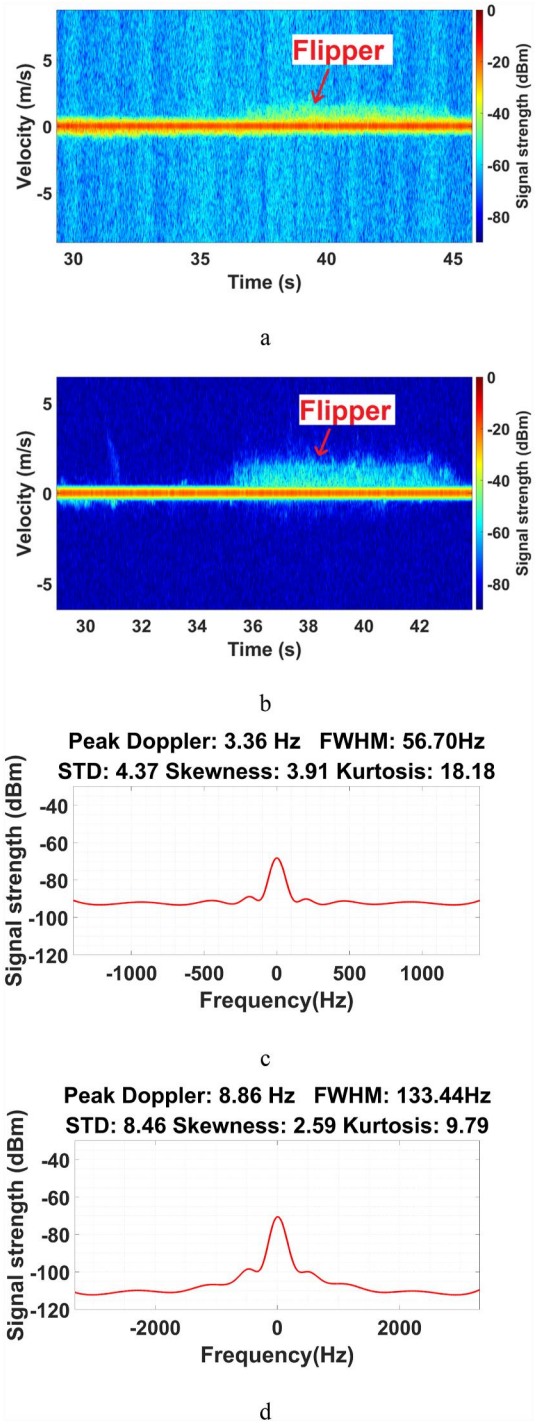

FIGURE 11 (a) 24 GHz spectrogram plots showing the Doppler signature of sea lion flipper, (b) 77 GHz spectrogram plot showing the Doppler signature of the same activity, (c) Corresponding 24 GHz Doppler spectra and central moment values, (d) Corresponding 77 GHz Doppler spectra and central moment values.

the collection of a large amount of data corresponding to the radar backscatter from three California sea lions performing different activities along with their natural behaviour. The RCS of different exposed parts of the sea lions has been calculated for HH and VV polarisations. The RCS values have a large variation, which is expected as they have been measured for different body parts and activities. No significant difference between the HH and VV signatures was found. Also, RCS values were quite comparable in general at both frequency bands. It is believed that the observed minor discrepancies are mainly due to a different proportion of the sea lion body being above the water at different instances. A brief Doppler analysis was also presented, mainly to point out the potential of the Doppler domain to be used for target classification feature extraction, by making a comparison with sea clutter data. For current research on sub-THz (W-band and above) radars for marine autonomous vessels, it is vital to obtain more experimental data of such animals. This will directly aid future work on automatic target recognition algorithm development.

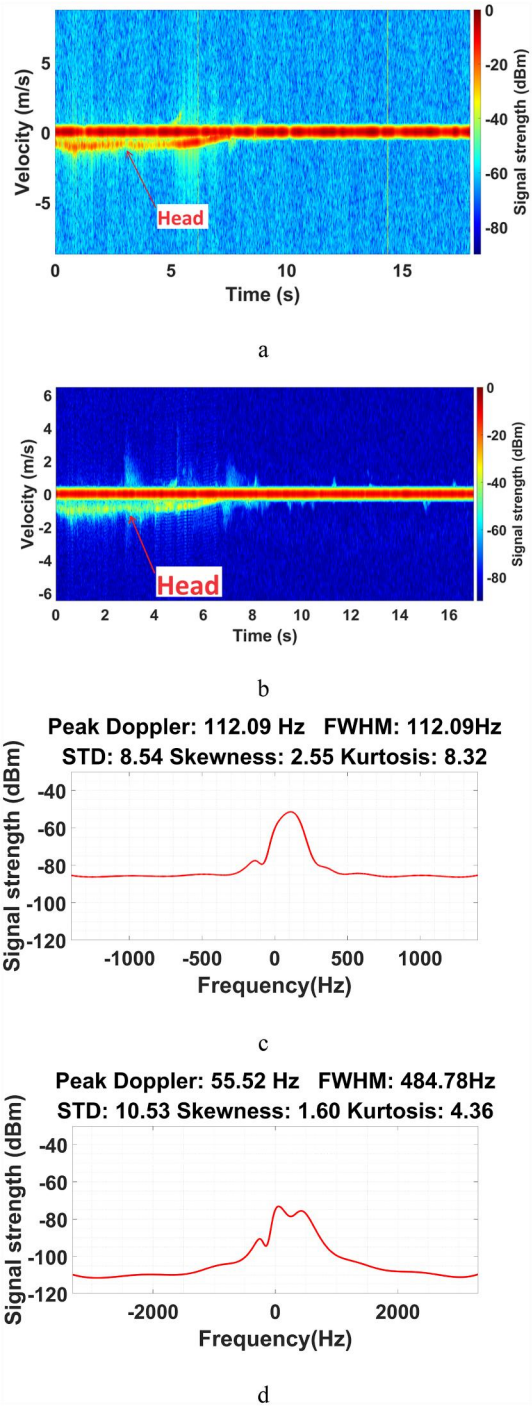

FIGURE 12 (a) 24 GHz spectrogram plots showing the Doppler signature of sea lion head, (b) 77 GHz spectrogram plot showing the Doppler signature of the same activity, (c) Corresponding 24 GHz Doppler spectra and central moment values, (d) Corresponding 77 GHz Doppler spectra and central moment values.

AUTHOR CONTRIBUTIONS

Samiur Rahman: Data curation; signal processing and data analysis; investigation, writing – main manuscript; writing – review & editing. **Aleksanteri B. Vattulainen**: Data curation; investigation; visualization; writing – review & editing. **Duncan A. Robertson**: Data curation; funding acquisition; investigation; supervision; writing – review & editing. **Ryan Milne**: Data curation; resources.

ACKNOWLEDGEMENTS

This work was supported by the UK Engineering and Physical Sciences Research Council under grant EP/S032851/1. The authors acknowledge Dr Douglas Gillespie and Simon Moss from the Sea Mammal Research Unit, St Andrews, for their support with successfully organising the experimental trial. Ethical approval for the experiments was granted by the University of St Andrews Bioethics committee.

CONFLICT OF INTEREST STATEMENT

The authors have no conflict of interest.

DATA AVAILABILITY STATEMENT

Data will be openly available in University of St Andrews public repository (Pure). DOI: https://doi.org/10.17630/ac0c6013-801c-45fd-92f2-ed1482523ade (will be activated later).

ORCID

Samiur Rahman https://orcid.org/0000-0002-5477-4218
Aleksanteri B. Vattulainen https://orcid.org/0000-0003-1898-600X
Duncan A. Robertson https://orcid.org/0000-0002-4042-2772

REFERENCES

1. Mein, S., Nebel, S.: The use of radar in the study of animal migration. https://www.nature.com/scitable/knowledge/library/the-use-of-radar-in-the-study-84825627/. Accessed 8 Sep 2023
2. Nathanson, F., Reilly, J.P., Cohen, M.N.: Radar Design Principles: Signal Processing and the Environment. New York (1969)
3. Deprospo, D.F., et al.: Radar-based Detection, Tracking and Speciation of Marine Mammals from Ships. Areté Associates project report (2004)
4. Forsyth, C.P.: Radar Detection of Marine Mammals. Areté Associates project report (2010)
5. Ward, K., Tough, R., Watts, S.: Sea Clutter: Scattering, the K Distribution and Radar Performance. Institution of Engineering and Technology (2013)
6. Anderson, S.J., Morris, J.T.: On the detection of marine mammals with ship-borne polarimetric microwave radar. In: OCEANS'10 IEEE Sydney, OCEANSSYD 2010, pp. 1–6 (2010)
7. McCann, D.L., Bell, P.S.: Observations and tracking of killer whales (Orcinus orca) with shore-based X-band marine radar at a marine energy test site. Mar. Mamm. Sci. 33(3), 904–912 (2017). https://doi.org/10.1111/mms.12395
8. Mingozzi, M., Salvioli, F., Serafino, F.: X-band radar for cetacean detection (focus on Tursiops truncatus) and preliminary analysis of their behavior. Rem. Sens. 12(3), 388 (2020). https://doi.org/10.3390/rs12030388
9. Rahman, S., et al.: Millimetre wave radar signatures of sea lions. In: International Conference on Radar Systems (2022)
10. Rahman, S., Robertson, D.A.: Coherent 24 GHz FMCW radar system for micro-Doppler studies. In: Proceedings of the SPIE 10633, Radar Sensor Technology XXII, vol. 10633, pp. 1–9 (2018)
11. Rahman, S., Robertson, D.A.: FAROS-E: a compact and low-cost millimeter wave surveillance radar for real time drone detection and classification. Proc. Int. Radar Symp. 2021, 1–6 (2021)

12. Richards, M.A.: Fundamentals of Radar Signal Processing. McGraw-Hill, New York (2005)
13. Skolnik, M.I.: Introduction to Radar Systems. McGraw Hill (2001)
14. Robertson, D.A., Brooker, G.M., Beasley, P.D.L.: Very low-phase noise, coherent 94GHz radar for micro-Doppler and vibrometry studies. In: Proceedings of the SPIE 9077, Radar Sensor Technology XVIII, vol. 9077, p. 907719 (2014)

How to cite this article: Rahman, S., et al.: Radar signatures of sea lions at K-band and W-band. IET Radar Sonar Navig. 1–11 (2023). https://doi.org/10.1049/rsn2.12498